MULTI-PERSON BREATHING RATE ESTIMATION USING TIME-REVERSAL ON WIFI PLATFORMS

Chen Chen⋆†*, Yi Han*⋆†*, Yan Chen*∗†*, and K.J. Ray Liu*⋆†

⋆ University of Maryland, College Park, MD 20742, USA
† Origin Wireless, Suite 1070, 7500 Greenway Center Drive, MD 20770, USA
∗ School of Electronic Engineering, University of Electronic Science and Technology of China
Email: {cc8834, yhan1990, kjrliu}@umd.edu⋆, eecyan@uestc.edu.cn∗

ABSTRACT

In this paper, we present TR-BREATH, a time-reversal (TR) based, contact-free, accurate breathing monitoring system capable of multi-person breathing rate estimation within a short period of time (e.g., around one minute) using off-the-shelf WiFi devices. TR-BREATH exploits the fine-grained channel state information (CSI) on WiFi devices to capture the minor variations caused by breathing. To amplify such variations, TR-BREATH projects CSI time series into TR resonating strength (TRRS) feature space and performs Root-MUSIC to extract candidates of breathing rates. Then, TR-BREATH performs affinity propagation to partition these candidates into clusters corresponding to the breathing of different people. Extensive experiment results in a typical indoor environment demonstrate that under an non-line-of-sight scenario, TR-BREATH achieves an accuracy of 98.5% in estimating the breathing rates of one person, and a mean accuracy of 96.9% averaging over the accuracies of 1 to 7 people.

Index Terms— Channel state information, time-reversal resonating strength, breathing rate estimation.

1. INTRODUCTION

Breathing is a crucial vital indicator of one's physical and psychological conditions. However, most breathing monitoring systems are invasive in that physical contact to the human body is a must. For instance, in hospitals, patients are required to wear nasal cannulas or wearable sensors, while in polysomnography, at least 22 wire attachments to the human body are required for the sleep study. These specialized medical devices are in general bulky and costly, introducing discomforts to patients, and limited to clinical usage only.

To overcome these shortcomings, contact-free systems are developed for in-home and long-term monitoring. Among them, visual-based methods and RF-based methods are very popular. The visual-based approaches extract the breathing patterns from the captured images and/or videos. In [1], Nam *et al.* propose a method utilizing the cameras on a smartphone to capture the chest and abdominal motions of the subject for breathing rate estimation. The drawback with the visual-based schemes is that they are only effective when the subject is located within the vision of the capturing device. Thus, they cannot estimate the breathing rate of a subject behind obstacles, e.g., a subject behind a wall.

On the other hand, methods based on radio frequency (RF) can sense the human breathing even in the presence of significant occlusions. Based on the techniques, they can be further classified into radar-based and WiFi-based. Doppler radars are often used in radar-based methods [2], which exploits the frequency shift for breathing rates estimation. More recently, Adib *et al.* propose a vital sign monitoring system using frequency modulated continuous radar (FMCW) [3] leveraging Universal Software Radio Peripheral (USRP) as the RF front-end. However, the requirement of dedicated hardware hinders the deployment of these approaches.

WiFi-based methods are infrastructure-free due to the ubiquity of wireless local area networks (WLANs). In [4], Abdelnasser *et al.* present UbiBreathe that uses received signal strength (RSS) for breathing estimation. Yet, it is accurate only when the device is very close to the chest of the user. Another exploitable information on WiFi devices is the channel state information (CSI), a fine-grained portrait of the environment that contains much richer information than RSS. In this regard, the breathing monitoring system proposed in [5] is one of the first few works that leverage CSIs for device-free breathing monitoring. However, it only shows the viability of breathing monitoring of 1 to 2 people.

In this work, we propose TR-BREATH, a contact-free system capable of highly accurate multi-person breathing monitoring within a short period of measurement. TR-BREATH leverages the time-reversal (TR) resonating strength (TRRS) calculated using CSIs and adopts Root-MUSIC [6] and affinity propagation [7] for breathing rate estimation. It is infrastructure-free by the utilization of commercial WiFi devices instead of the dedicated hardware used in [2, 3, 8], and it can monitor multiple people under non-line-of-sight (NLOS) scenarios accurately even when both WiFi devices are placed outside the room to be monitored, while most of

the related works need at least one WiFi device in the same room with the people. Extensive experiment results in an office environment demonstrate that TR-BREATH achieves a mean accuracy of 98.5% with one person and an accuracy of 96.9% averaging over 1 to 7 people in the same room.

The rest of the paper is organized as follows. Section 2 presents a model that incorporates the impact of breathing on CSIs and introduces the time-reversal technique as well as the Root-MUSIC algorithm. Section 3 elaborates on the algorithm of TR-BREATH. Section 4 demonstrates the experiment results. Finally, conclusions are drawn in Section 5.

2. THEORETICAL FOUNDATION

2.1. Impact of Breathing on CSIs

CSI is reported as a vector in frequency domain given by $\mathbf{H} = \begin{bmatrix} H_0 & \cdots & H_k & \cdots H_{N-1} \end{bmatrix}^{\mathsf{T}}$, where $H_k = |H_k|e^{j\angle H_k}$ is the complex gain on subcarrier k with $\angle x$ denoting the angle of argument x in radians, N is the total number of subcarriers, and $(\cdot)^{\mathsf{T}}$ is the transpose operator.

Given L multipaths components (MPCs) with a delay profile $\{\tau_\ell\}_{\ell=1,2,\cdots,L}$ and a gain profile $\{g_\ell\}_{\ell=1,2,\cdots,L}$, the *normalized CSI* $\underline{\mathbf{H}}$ is written as [9]

$$\underline{\mathbf{H}} = \mathbf{\Gamma}(\alpha,\beta) \begin{bmatrix} \mathbf{\Phi}_1 & \mathbf{\Phi}_2 & \cdots & \mathbf{\Phi}_\ell & \cdots & \mathbf{\Phi}_L \end{bmatrix} \mathbf{g}, \quad (1)$$

where $||\underline{\mathbf{H}}||_2 = 1$ and $||\cdot||_2$ is the $\mathcal{L}2$ norm, $\mathbf{\Phi}_\ell$ is the basis vector for the ℓ-th multipath given as $\begin{bmatrix} 1 & \Phi_\ell & \cdots & \Phi_\ell^{N-1} \end{bmatrix}^{\mathsf{T}}$ with $\Phi_\ell = e^{-j2\pi\tau_\ell\Delta f}$, Δf is the subcarrier spacing, and $\mathbf{g} = \begin{bmatrix} g_1 & g_2 & \cdots & g_L \end{bmatrix}^{\mathsf{T}}$ is the complex gain vector for the L multipaths. $\mathbf{\Gamma}(\alpha,\beta)$ is a diagonal matrix representing the additional phase rotation due to synchronization errors with its (k,k)-th entry given as $[\mathbf{\Gamma}(\alpha,\beta)]_{k,k} = e^{-j2\pi\frac{\alpha+\beta k}{N}}$ [10]. Here, α and β are the initial and linear phase distortions, respectively.
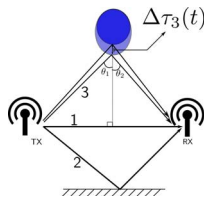
Fig. 1: Impact of breathing on the multipath components.

To study how breathing affects CSI, we adopt an intuitive channel model consisting of 3 MPCs with one person breathing as shown in Fig. 1, where (i) MPC 1 is a LOS path (ii) MPC 2 is a static reflection path (iii) MPC 3 is a dynamic reflection path that traverses the chest of the human body. The delay of MPC 3 is given by $\tau_3(t) = \tau_{3,0} + \Delta\tau_3(t)$, where $\tau_{3,0}$ is the average delay of MPC 3, and $\Delta\tau_3(t)$ is the miniature path delay variation of MPC 3 with period T due to human breathing such that $\Delta\tau_3(t) = \Delta\tau_3(t+nT)$ for integer n. θ_1

and θ_2 are the incidence and reflection angles to and from the human body, respectively. Hence, the CSI incorporating the impact of chest movement can be written as

$$\underline{\mathbf{H}}(t) = \mathbf{\Gamma}(\alpha(t),\beta(t))\left[\underbrace{\begin{bmatrix} \mathbf{\Phi}_1 & \mathbf{\Phi}_2 & 0 \end{bmatrix}\begin{bmatrix} g_1 & g_2 & 0 \end{bmatrix}^{\mathsf{T}}}_{\mathbf{C}} + \mathbf{\Phi}_3(t)g_3 \right],$$

$$(2)$$

where $\alpha(t)$ and $\beta(t)$ are the time-varying synchronization errors, $\mathbf{\Phi}_3(t) = \begin{bmatrix} 1 & \cdots & \Phi_3^k(t) & \cdots & \Phi_3^{N-1}(t) \end{bmatrix}^{\mathsf{T}}$ with $\Phi_3(t) = e^{-j2\pi\tau_3(t)\Delta f}$, and $\mathbf{C}$ is the static component of $\underline{\mathbf{H}}(t)$.

2.2. Feature Extraction using Time-Reversal and Root-MUSIC

The TRRS can be considered as a measure of similarity between two channel impulse responses (CIRs) in time domain [11]. It is given as $\gamma[\mathbf{h},\mathbf{h}'] = \max_i |(\mathbf{h}*\mathbf{g})[i]|$, where $\mathbf{h}$ and $\mathbf{h}'$ are two normalized CIRs with $||\mathbf{h}||_2 = ||\mathbf{h}'||_2 = 1$, $*$ stands for convolution, and $\mathbf{g}$ is the time-reversed and conjugate version of $\mathbf{h}'$.

By virtue of the property that convolution in time domain can be written into inner product in frequency domain and assuming that $\mathbf{\Gamma}(\alpha(t),\beta(t))$ is mitigated, the TRRS in frequency domain is defined as $\gamma[\underline{\mathbf{H}},\underline{\mathbf{H}}'] = \underline{\mathbf{H}}^{\dagger}\underline{\mathbf{H}}'$, where $(\cdot)^{\dagger}$ is the Hermitian operator and $\gamma[\underline{\mathbf{H}},\underline{\mathbf{H}}'] \in [0,1]$. Denote the two CSIs captured at the n-th and m-th time instance with a sampling interval of T_s as $\underline{\mathbf{H}}(nT_s)$ and $\underline{\mathbf{H}}(mT_s)$ respectively, for a fixed m, the TRRS between them is approximated by

$$\gamma[\underline{\mathbf{H}}(nT_s),\underline{\mathbf{H}}(mT_s)] \approx \mathbf{C}'^{\dagger}\mathbf{C}' + \mathbf{\Phi}_3^{\dagger}(mT_s)\mathbf{C}'g_3'^* + u[n] \quad (3)$$

where $u[n] = \mathbf{C}'^{\dagger}\mathbf{\Phi}_3(nT_s)g_3'$ is complex periodic and can be decomposed into its Fourier series expression given as $\overline{u} + \rho e^{j2\pi fnT_s} + \eta[n]$. Here, $f = 1/T$, $\overline{u}$ is the nominal value of $u[n]$, ρ is the Fourier series coefficient for the first-order term f, and $\eta[n]$ is the residual term composed by high-order harmonics. Thus, $\gamma[\underline{\mathbf{H}}(nT_s),\underline{\mathbf{H}}(mT_s)]$ can be written into $\rho e^{j2\pi fnT_s} + \eta'[n]$, where $\eta'[n] = \eta[n] + \overline{u} + \mathbf{C}'^{\dagger}\mathbf{C}' + \mathbf{\Phi}_3^{\dagger}(mT_s)\mathbf{C}'g_3'^*$. The derivations can be generalized into K people breathing with frequencies $\{f_i\}_{i=1,\cdots,K}$, with $\gamma[\underline{\mathbf{H}}(nT_s),\underline{\mathbf{H}}(mT_s)] = \overline{\mu} + \sum_{i=1}^{K}\rho_i e^{j2\pi f_i nT_s} + \eta'[n]$.

Finally, given M normalized CSI measurements $\underline{\mathbf{H}}(nT_s)$ with $n = 0,1,\cdots,M$, we can formulate the $M \times M$ TRRS matrix $\mathbf{R}$ that can be expressed concisely as

$$\mathbf{R} = \begin{bmatrix} \phi_0 & \phi_1 & \phi_2 & \cdots & \phi_K \end{bmatrix} \mathbf{A} + \boldsymbol{\eta}, \quad (4)$$

where $\phi_k = \begin{bmatrix} 1 & \psi_k & \psi_k^2 & \cdots & \psi_k^{M-1} \end{bmatrix}^{\mathsf{T}}$ is the *steering vector* [12] associated with the k-th breathing rate with $\psi_k = e^{j2\pi f_k T_s}$ and $\psi_0 = \begin{bmatrix} 1 & 1 & \cdots & 1 \end{bmatrix}^{\mathsf{T}}$. In (4), $\mathbf{A}$ contains the Fourier series coefficients, and $\boldsymbol{\eta}$ contains the remaining terms including the harmonics and the static terms.

Given (4), $\{f_i\}_{i=1,\cdots,K}$ can be obtained via Root-MUSIC, a high-resolution spectral analyzer widely adopted in the

field of signal processing [6]. Assuming the signal subspace size as p, Root-MUSIC performs eigenvalue decomposition on $\mathbf{R}$ and partitions the eigenvalues into signal and noise eigenvalues. The associated eignvectors with respect to the noise eigenvalues are then assembled into the eigenmatrix $\mathbf{Q}$. Writing the steering vector ϕ into $\begin{bmatrix} 1 & z^{-1} & z^{-2} & \cdots & z^{-(M-1)} \end{bmatrix}^{\mathsf{T}}$ with $z = e^{-j2\pi f T_s}$, Root-MUSIC solves the polynomial $\sum_{m=0}^{E-1} \sum_{n=0}^{E-1} z^{n-m} [\mathbf{U}]_{m,n} = 0$ where $E = M - p$ and $[\mathbf{U}]_{m,n}$ is the (m,n)-th entry of $\mathbf{U} = \mathbf{Q}\mathbf{Q}^{\dagger}$. The p solutions of the polynomial $\{\hat{z}_i\}_{i=1,\cdots,p}$ are then translated into the breathing rate estimations measured in breath-per-minute (BPM), denoted by $\{\hat{f}_i\}_{i=1,\cdots,p}$ where $\hat{f}_i = 60 \times \frac{\angle[\hat{z}_i]}{2\pi T_s}$. When $p = K + 1$, TR-BREATH produces the breathing rate estimations for all of the K people after discarding the dummy solution ψ_0.

3. ALGORITHM
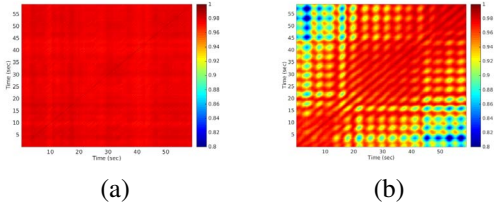
Fig. 2: TRRS matrices with (a) no people (b) 2 people.
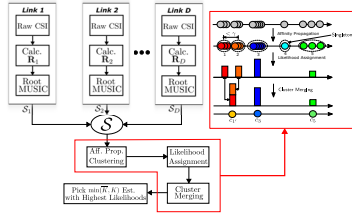
Fig. 3: Overview of the proposed architecture.

The foundation of TR-BREATH is built upon the observation that breathing introduces distinguishable patterns into the TRRS matrix, which is visualized in Fig. 2 with TRRS matrix calculated from CSIs measured with no one and two people in the same room, respectively. This observation motivates us to develop TR-BREATH which extracts useful information from the TRRS matrix.

Fig. 3 depicts the architecture of TR-BREATH. For each link d out of D total links on a multi-antenna WiFi platform, TR-BREATH normalizes and calculates the TRRS matrix $\mathbf{R}$ using CSIs captured within a time window of W seconds, i.e., $\{\underline{\mathbf{H}}(iT_s)\}_{i=0,\cdots,\lfloor(W-1)/T_s\rfloor}$, where $\lfloor \cdot \rfloor$ denotes the floor operator. To compensate the synchronization error $\mathbf{\Gamma}(\alpha(t), \beta(t))$, we calculate the (m,n)-th entry of ma-

trix $\mathbf{R}$ as $[\mathbf{R}]_{m,n} = [\mathbf{\Gamma}(0, -\beta^{\star})\underline{\mathbf{H}}(mT_s)]^{\dagger} \underline{\mathbf{H}}(nT_s)$, where $\beta^{\star} = \arg\max_{\beta} \left| [\mathbf{\Gamma}(0, -\beta^{\star})\underline{\mathbf{H}}(mT_s)]^{\dagger} \underline{\mathbf{H}}(nT_s) \right|$.

TR-BREATH performs Root-MUSIC on $\mathbf{R}$ with signal subspace p to obtain p candidates of breathing rates. Then, TR-BREATH shifts the time window by P seconds and computes $\mathbf{R}$ with $\{\underline{\mathbf{H}}(iT_s)\}_{i=\lfloor P/T_s\rfloor,\cdots,\lfloor(P+W-1)/T_s\rfloor}$. Therefore, given a total of M CSIs, TR-BREATH formulates a total of $V_{\max} = \lfloor (MT_s - W)/P \rfloor$ TRRS matrix $\mathbf{R}$ and thus $pV_{\max}$ candidates of breathing rates per link. All breathing estimation candidates of all D links are then fused into the set $\mathcal{S}$ for further processing.

Because that the human breathing rate is confined in a certain range, say, $[f_{\min}, f_{\max}]$ BPM, after obtaining $\mathcal{S}$, TR-BREATH sifts $\mathcal{S}$ by discarding candidates not in $[f_{\min}, f_{\max}]$. Then, it performs affinity propagation clustering [7] on all elements in $\mathcal{S}$. The clustering requires a similarity measure between any two candidates $\hat{f}_i$ and $\hat{f}_j$, which is given as $e^{-|\hat{f}_i - \hat{f}_j|}$ in this work.

Assuming that affinity propagation returns U clusters. For the i-th cluster, TR-BREATH evaluates the population p_i, variance v_i, and centroid c_i. p_i and v_i are normalized as $\overline{p}_i = \frac{p_i}{\sum_{i=1}^{U} p_i}$ and $\overline{v}_i = \frac{v_i}{\sum_{i=1}^{U} v_i}$. The likelihood of cluster i, denoted as l_i, is calculated as (i) $l_i = 0$ if $v_i = 0, p_i = 1$, i.e., cluster i is a singleton. (ii) Otherwise, $l_i = m_i / \sum_{i=1}^{U} m_i$ with $m_i = e^{\omega_p \overline{p}_i - \omega_v \overline{v}_i - \omega_c c_i}$, and $(\omega_p, \omega_v, \omega_c)$ are positive factors compensating the different scales of $(\overline{p}_i, \overline{v}_i, c_i)$

Since the breathing rates are evaluated for each time window and for each link independently, it is likely that breathing rate estimations for the same person differ slightly, yielding several closely-spaced clusters. Thus, TR-BREATH measures the distances between centroids and merges clusters with distances smaller than a threshold, named as the merging radius and denoted by γ. As an example, in Fig. 3, TR-BREATH merges cluster 1 and 2 into the new cluster $1'$ and recalculates the population as $\overline{p}_{1'} = \overline{p}_1 + \overline{p}_2$, and evaluates $\overline{v}_{1'}$ as the variance of the new cluster. The cluster centroid $1'$ is updated as $c_{1'} = \frac{l_1 c_1 + l_2 c_2}{l_1 + l_2}$, i.e., average of c_1 and c_2 weighted by l_1 and l_2. The likelihood of cluster $1'$ is given by $l_{1'}$ calculated using $(\overline{p}_{1'}, \overline{v}_{1'}, c_{1'})$.
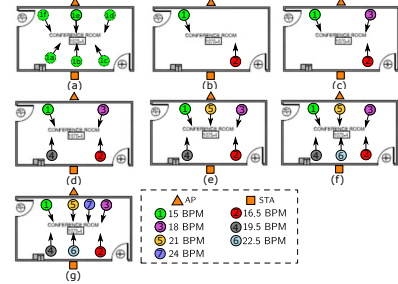
Fig. 4: Experiment settings.

Finally, assuming a total of $\overline{K}$ clusters after merging
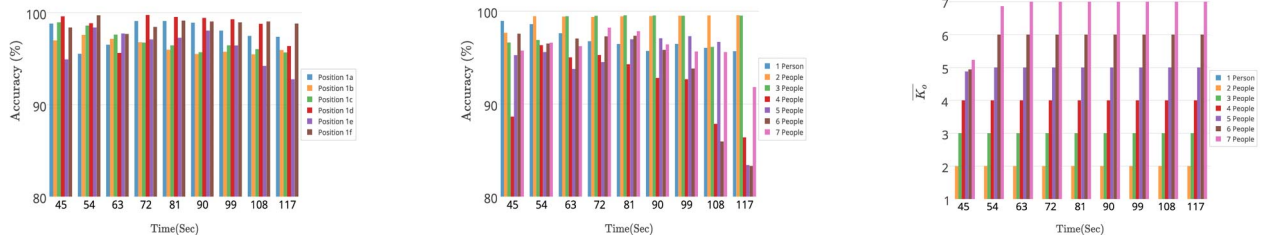
(a) Accuracy under NLOS 1 person scenario under $W = 45s$ and various V.

(b) Accuracy under NLOS $1 \sim 7$ people scenario under $W = 45s$ and various V.

(c) $\overline{K_o}$ under $W = 45s$ and various V.

Fig. 5: TR-BREATH performances under NLOS single person and multiple people scenarios, with $W = 45s$ and different V.

and that K is known, TR-BREATH sorts the centroids $\{c_i\}_{i=1,\cdots,\overline{K}}$ by the descending order of their likelihoods, and outputs $K_o = \min(\overline{K}, K)$ centroids with the highest likelihoods as the breathing rate estimations denoted as $\{\hat{f}_i\}_{i=1,\cdots,K_o}$.

4. EXPERIMENT RESULTS

The experiments are conducted in one conference room with size 8m×5m in a typical office building during normal business hours. We use one pair of off-the-shelf WiFi devices to capture CSIs. One of the WiFi devices works as the access point (AP), while the other works as the station (STA). Both AP and STA are equipped with 3 omnidirectional antennas, leading to $D = 9$ total links. The WiFi devices are placed in an NLOS setting with their direct link blocked by two walls as shown in Fig. 4. The center frequency is configured as 5.765 GHz (WiFi channel 153).

Seven participants are invited to take the experiments. To obtain baselines, they are asked to breathe in synchronous with metronomes. Two experiments are conducted: (i) one person seated at 6 different locations with different facing orientations in the conference room, labelled as 1a to 1f in Fig. 4(a) (ii) Up to 7 people seated in the same room as shown in Fig. 4(a)-(g). The facing orientations and ground-truth breathing rates for all participants are shown in Fig. 4 as well.

Each experiment lasts for 2 minutes. The Root-MUSIC signal subspace order p is 10, γ is 1 BPM, $f_{\min} = 10$ BPM, and $f_{\max} = 50$ BPM. The CSI measurement interval T_s is 0.1s, and W is 45s with $P = 4.5s$. The maximum number of windows is $V_{\max} = 17$, and the total time of CSI measurement with V windows is $T_{\text{tot}} = 45 + (V-1) \times 4.5$ seconds.

We evaluate the performance of TR-BREATH using two metrics: accuracy and average resolvable number of people. Given estimated BPM $\hat{\mathbf{f}} = [\hat{f}_1, \cdots, \hat{f}_{K_o}]$ and ground-truth BPM $\mathbf{f} = [f_1, f_2, \cdots, f_K]$, the accuracy is calculated by $\text{Acc}[\hat{\mathbf{f}}, \mathbf{f}] = 1 - \frac{1}{K_o} \sum_{i=1}^{K_o} \left| \frac{\hat{f}_i - f_i}{f_i} \right|$. On the other hand, the average of K_o, denoted as $\overline{K_o}$, signifies how many people

on average TR-BREATH can resolve. For instance, $\overline{K_o} = 4, K = 5$ implies a missing detection of 1 person on average, while $\overline{K_o} = 5, K = 5$ indicates that TR-BREATH resolves all 5 breathing rates on average.

The accuracy performances under NLOS with one person at different locations are shown in Fig. 5(a) under different V and thus various T_{tot}. It can be seen that TR-BREATH achieves $\geq 90\%$ accuracy for all cases. Specifically, TR-BREATH achieves an accuracy of 98.5% under $T_{\text{tot}} = 63s$. Therefore, we conclude that TR-BREATH is insensitive to the positions and facing orientations of people.

The accuracy and $\overline{K_o}$ are illustrated in Fig. 5(b), (c) respectively under the NLOS multi-person scenario. The accuracy under $T_{\text{tot}} = 63s$ is 97.6%, 99.4%, 99.5%, 95.0%, 93.8%, 97.1%, and 96.2% under 1, 2, 3, 4, 5, 6, and 7 people scenarios respectively, producing a mean accuracy of 96.9% by averaging over $K = 1 \sim 7$. Fig. 5(c) shows that $K_o = K$ after $T_{\text{tot}} = 63s$, implying that TR-BREATH resolves enough breathing rates when $T_{\text{tot}} \geq 63s$. Interestingly, the accuracy degrades when $T_{\text{tot}} \geq 108s$ for $K \geq 4$ while $\overline{K_o} = K$. This can be justified by that the human breathing rate can hardly be kept constant in a long monitoring time. In this sense, T_{tot} should be carefully chosen to guarantee the optimal performance.

5. CONCLUSION

In this paper, we present TR-BREATH, a breathing monitoring system capable of multi-person monitoring using off-the-shelf WiFi devices. TR-BREATH exploits TRRS to extract breathing features and formulates breathing rate estimations via Root-MUSIC and affinity propagation. Experiment results demonstrate that with 63 seconds of measurements in an NLOS scenario, TR-BREATH achieves an accuracy of 98.5% for one person and a mean accuracy of 96.9% averaging over the accuracies with 1 to 7 people. With ubiquitous WiFi, TR-BREATH would have a huge impact on future medical applications by providing real-time, in-home, multi-person, and contact-free medical services.

6. REFERENCES

[1] Y. Nam, Y. Kong, B. Reyes, N. Reljin, and K. H. Chon, "Monitoring of heart and breathing rates using dual cameras on a smartphone," *PloS one*, vol. 11, no. 3, 2016.

[2] B.-K. Park, S. Yamada, O. Boric-Lubecke, and V. Lubecke, "Single-channel receiver limitations in doppler radar measurements of periodic motion," in *Radio and Wireless Symposium, 2006 IEEE*, pp. 99–102, Jan 2006.

[3] F. Adib, H. Mao, Z. Kabelac, D. Katabi, and R. C. Miller, "Smart homes that monitor breathing and heart rate," in *Proceedings of the 33rd Annual ACM Conference on Human Factors in Computing Systems*, CHI '15, (New York, NY, USA), pp. 837–846, ACM, 2015.

[4] H. Abdelnasser, K. A. Harras, and M. Youssef, "Ubibreathe: A ubiquitous non-invasive wifi-based breathing estimator," in *Proceedings of the 16th ACM International Symposium on Mobile Ad Hoc Networking and Computing*, MobiHoc '15, (New York, NY, USA), pp. 277–286, ACM, 2015.

[5] J. Liu, Y. Wang, Y. Chen, J. Yang, X. Chen, and J. Cheng, "Tracking vital signs during sleep leveraging off-the-shelf wifi," in *Proceedings of the 16th ACM International Symposium on Mobile Ad Hoc Networking and Computing*, MobiHoc '15, pp. 267–276, 2015.

[6] B. D. Rao and K. V. S. Hari, "Performance analysis of root-music," *IEEE Transactions on Acoustics, Speech, and Signal Processing*, vol. 37, pp. 1939–1949, Dec 1989.

[7] B. J. Frey and D. Dueck, "Clustering by passing messages between data points," *Science*, vol. 315, p. 2007, 2007.

[8] N. V. Rivera, S. Venkatesh, C. Anderson, and R. M. Buehrer, "Multi-target estimation of heart and respiration rates using ultra wideband sensors," in *Signal Processing Conference, 2006 14th European*, pp. 1–6, Sept 2006.

[9] M. Kotaru, K. Joshi, D. Bharadia, and S. Katti, "SpotFi: Decimeter level localization using WiFi," in *Proceedings of the 2015 ACM Conference on Special Interest Group on Data Communication*, SIGCOMM '15, (New York, NY, USA), pp. 269–282, ACM, 2015.

[10] M. Speth, S. Fechtel, G. Fock, and H. Meyr, "Optimum receiver design for wireless broad-band systems using OFDM—Part I," *Communications, IEEE Transactions on*, vol. 47, pp. 1668–1677, Nov 1999.

[11] Z.-H. Wu, Y. Han, Y. Chen, and K. J. R. Liu, "A time-reversal paradigm for indoor positioning system," *Vehicular Technology, IEEE Transactions on*, vol. 64, pp. 1331–1339, April 2015.

[12] M. H. Hayes, *Statistical Digital Signal Processing and Modeling*. New York, NY, USA: John Wiley & Sons, Inc., 1st ed., 1996.